Environmental Science & Technology

Article

pubs.acs.org/est

Modeling Ozone Removal to Indoor Materials, Including the Effects of Porosity, Pore Diameter, and Thickness

Elliott T. Gall,[†] Jeffrey A. Siegel,[‡] and Richard L. Corsi*[,§]

[†]Nanyang Technological University and Berkeley Education Alliance for Research in Singapore, 1 Create Way #11-01 Create Tower, Singapore, 138602

[‡]Department of Civil Engineering and Dalla Lana School of Public Health, University of Toronto, 35 St. George St., Toronto, Ontario M5S 1A4, Canada

[§]Department of Civil, Architectural and Environmental Engineering, Cockrell School of Engineering, The University of Texas at Austin, 1 University Station C1786, Austin, Texas 78712, United States

Supporting Information

ABSTRACT: We develop an ozone transport and reaction model to determine reaction probabilities and assess the importance of physical properties such as porosity, pore diameter, and material thickness on reactive uptake of ozone to five materials. The one-dimensional model accounts for molecular diffusion from bulk air to the air−material interface, reaction at the interface, and diffusive transport and reaction through material pore volumes. Material-ozone reaction probabilities that account for internal transport and internal pore area, γ_{ipa}, are determined by a minimization of residuals between predicted and experimentally derived ozone concentrations. Values of γ_{ipa} are generally less than effective reaction probabilities (γ_{eff}) determined previously, likely because of the inclusion of diffusion into substrates and reaction with internal surface area (rather than the use of the horizontally projected external material areas). Estimates of γ_{ipa} average 1×10^{-7}, 2×10^{-7}, 4×10^{-5}, 2×10^{-5}, and 4×10^{-7} for two types of cellulose paper, pervious pavement, Portland cement concrete, and an activated carbon cloth, respectively. The transport and reaction model developed here accounts for observed differences in ozone removal to varying thicknesses of the cellulose paper, and estimates a near constant γ_{ipa} as material thickness increases from 0.02 to 0.16 cm.

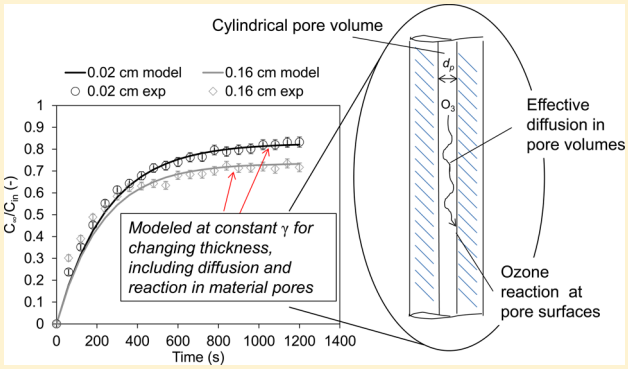

INTRODUCTION

There are known health consequences associated with ozone exposure.[1−4] Indoor exposures contribute substantially to total exposure, and may explain variations in ozone mortality coefficients across cities.[5,6] High indoor surface area to volume ratios compared with outdoor environments result in ozone reactions with indoor materials.[7−9] Indoor surfaces with strong sink effects may enable materials to be used as passive pollutant controls to suppress indoor concentrations of pollutants like ozone.[9−14] Measurements and empirical estimates of material-ozone interactions are well characterized,[15−18] as are secondary emissions resulting from ozone reactions to a range of materials.[8,13,19,20]

Previous studies of indoor material-ozone interactions typically combine the impact of material properties, for example, porosity, into transport and reaction phenomena described by a single parameter, the ozone deposition velocity, v_d (m h^{-1}) as summarized and discussed by Nazaroff et al.[21] Deposition velocities are often then employed in resistance uptake theory, for which physical and chemical processes occurring in a gas-surface system are treated in terms of resistances in series. Resistance uptake theory describes v_d in terms of a transport-limited deposition velocity, v_t (m h^{-1}), a characteristic of the fluid mechanics of a space, and the reaction probability, γ (−), the fractional likelihood of a reaction given a collision between a surface and reactive pollutant in air. This relationship is described by eq 1:

$$\frac{1}{v_d} = \frac{1}{v_t} + \frac{4}{<v> \gamma} \quad (1)$$

where $<v>$ = Boltzmann velocity, m h^{-1}, and other terms are as defined above.

Mass balance models are generally used to determine v_d by normalizing ozone loss rates by the aerial projection of the surface of a material, and this area is often the only physical descriptor of the material. As can be observed by eq 1,

Received: January 2, 2015
Revised: March 3, 2015
Accepted: March 6, 2015
Published: March 6, 2015

DOI: 10.1021/acs.est.5b00023
Environ. Sci. Technol. 2015, 49, 4398−4406

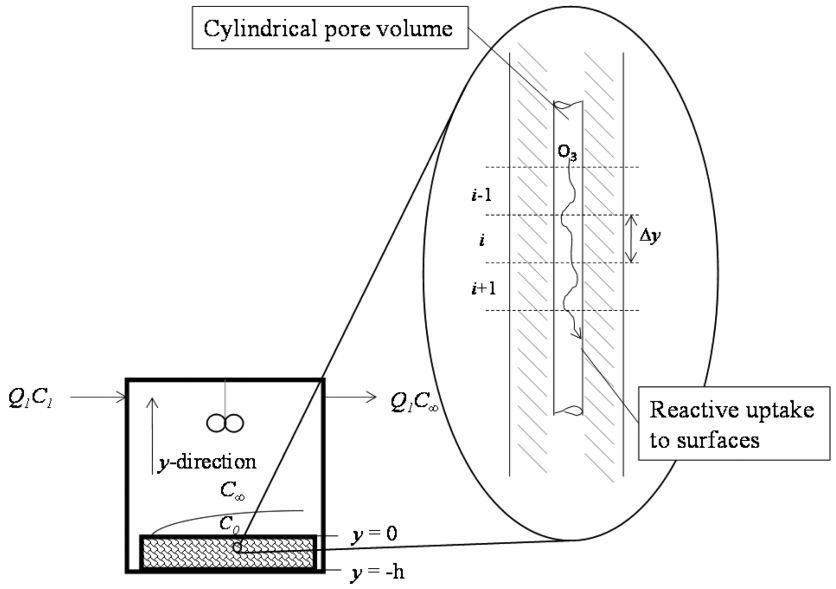

Figure 1. Model schematic for ozone transport and reaction within porous materials.

calculating γ from v_d results in the propagation of assumptions from estimation of v_d into the reaction probability. Models that incorporate material characteristics in this implicit way limit the ability to model reactive uptake of ozone to porous materials, where internal transport and reaction affect bulk ozone concentrations.[22]

Porous materials play an important role in indoor air pollution control. Activated carbon is known to adsorb pollutants like VOCs and react with ozone,[23,24] porous filters are used to remove particulate matter from air,[25] and porous zeolites can act as a catalyst for the oxidation of VOCs in the presence of an oxidizer like ozone.[26] Fundamental models describing the transport of pollutants in materials exist[27,28] and can address porous diffusion and adsorption/desorption processes (e.g., Marion et al.[29]). However, these models generally aim to describe indoor materials as sources or sinks of volatile organic compounds (VOCs) or semivolatile organic compounds (SVOCs). While several models of ozone transport in porous media exist,[30−32] Morrison and Nazaroff[33] developed a transport and reaction model most relevant to the work in this investigation. They characterized interior surface geometries of carpet, diffusive mass transport within the carpet itself, and reaction between ozone and carpet fibers and carpet backing. They noted that the geometry of carpet is an example of a broader class of materials in indoor environments in which material morphology and interior intricacy may affect reaction rates.

In this work, we build on the mechanistic approach taken by others, and attempt to decouple material physical properties and transport phenomena in parametrizations of ozone reactions with indoor surfaces. This research complements a previous investigation by Gall et al.[34] that characterized material physical properties of five test materials, and that highlighted challenges in estimating reaction probabilities when material porosity, pore size, thickness, and effective diffusion coefficient are varied. Here, we present a transport and reaction model derived from first-principles, and that uses previous parametrizations of material physical properties as inputs.[34] Estimates of reaction probabilities determined with this model, defined as γ_{ipa} to indicate the model's incorporation of internal pore area (IPA) are compared to estimates made with resistance uptake theory (eq 1) using aerial projections of surface area (effective reaction probabilities, γ_{eff}). The implications of model results for ozone control in indoor spaces is also presented and discussed.

MATERIALS AND METHODS

Five test materials were selected based on previous work characterizing physical properties and effective diffusion coefficients.[34] The five materials were cellulose filter papers of varying manufacturer-specified particle retention diameter (WF14 at 20−25 μm and WF15 at 2.5 μm), pervious pavement (PP), Portland cement concrete (PCC), and activated carbon cloth (ACC). Materials were chosen to maintain the same (WF14 and WF15) or similar (PP and PCC) chemical composition to isolate and assess the impact of physical properties on ozone removal. ACC was included due to its unique combination of high porosity, high effective diffusion coefficient, and large internal surface area. As described by Gall et al.,[34] and summarized in Supporting Information Table S1, inputs to the model developed here, including material porosity, pore size distributions, and median pore diameters (by volume) were measured using mercury intrusion porosimetry (MIP), while effective diffusion coefficients were measured with a dual-chamber diffusion apparatus. Uptake of ozone to materials was determined in an 11.4 L electropolished stainless steel chamber, operating at an air exchange rate of 11.7 $\pm$ 0.1 h^{-1}.

Model Development. The transport and reaction model was developed to independently account for the impact of porosity, pore size, material thickness, and the material-ozone effective diffusion coefficient on reactive uptake of ozone. A schematic illustrating the model framework is shown in Figure 1. A volume of a porous material with thickness h (m) was placed in a well-mixed experimental chamber at constant temperature and relative humidity, with constant ozone concentration C_1 (ppb) entering the chamber at constant flow rate Q_1 (m^3 h^{-1}). All boundaries of the material, with the exception of the upper surface, were encased in a PTFE barrier such that they were impenetrable by fluid flow within the

DOI: 10.1021/acs.est.5b00023
Environ. Sci. Technol. 2015, 49, 4398−4406

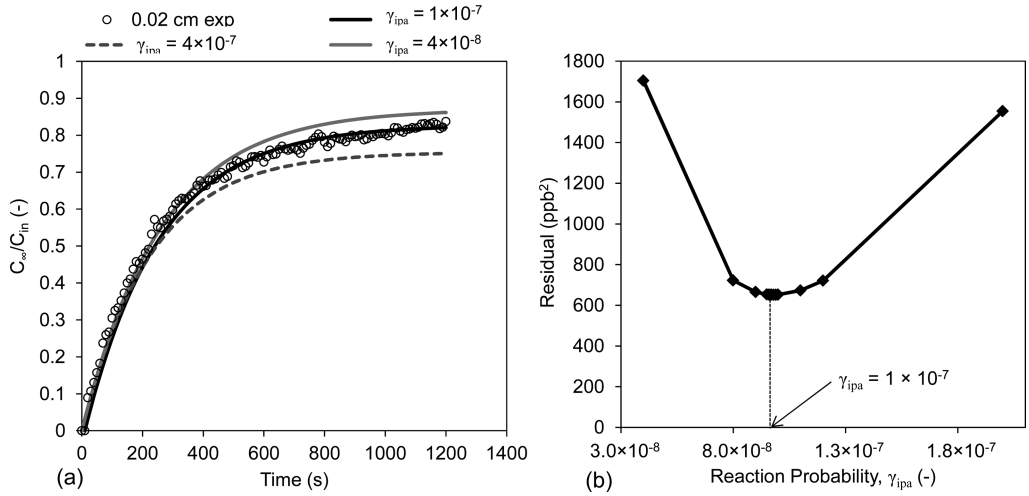

Figure 2. Example illustrating minimization of total residual for 0.02 cm condition of 20−25 μm retention cellulose filter paper (WF14). Plot (a) shows the modeled data plotted with experimental data and the visual confirmation of improved fit at $\gamma_{ipa} = 1 \times 10^{-7}$. Higher γ_{ipa} result in underprediction of ozone concentrations in chamber air, whereas lower γ_{ipa} result in overprediction. Plot (b) shows the quantitative confirmation of this as the total residual is minimized across the γ_{ipa} modeled for this material at this condition.

chamber and essentially unreactive with ozone. The ozone present in the air above the material is assumed to have a bulk concentration C_∞ (ppb), and to migrate by molecular diffusion through the concentration boundary layer and reach the surface of the material at concentration C_0 (ppb).

A mass balance on ozone in chamber air gives eq 2:

$$V\frac{\partial C_\infty}{\partial t} = Q_1C_1 - Q_1C_\infty - v_{d,w}A_wC_\infty - v_{d,m}(1-\varepsilon)A_mC_0 - D_e\frac{\partial C}{\partial y}\bigg|_{y=0}\varepsilon A_m \quad (2)$$

where Q_1, C_1, C_0, and C_∞ are as previously defined, V is the chamber volume (m^3), t is time (s), $v_{d,w}$ is the deposition velocity to the surfaces of the chamber (m h^{-1}), A_w is the area of chamber walls (m^2), $v_{d,m}$ is the deposition velocity to the experimental material (m h^{-1}), ε is the material porosity (−), A_m is the projected area of the top surface of the material (m^2), D_e is the effective diffusion coefficient of ozone in the material (m^2 h^{-1}), and y is the axial distance along the pore (m), as shown in Figure 1. Concentration boundary layers above the material (shown in Figure 1) and above chamber surfaces (not pictured) were assumed to develop instantaneously, therefore $v_{d,w}$ and $v_{d,m}$ are assumed constant in time.

A mass balance on ozone within an assumed cylindrical control volume i of a material with cylindrical pores can be written as eq 3:

$$\varepsilon A_{CV}\Delta y\frac{\partial C_i}{\partial t} = Q_iC_{i-1} - Q_iC_i + D_e\frac{\partial C}{\partial y}\bigg|_{i1/2}A_{CV}\varepsilon - D_e\frac{\partial C}{\partial y}\bigg|_{i1/2}A_{CV}\varepsilon - v_dC_iP\Delta y \quad (3)$$

where A_{CV} is the area of projection in the axial (y) direction of a cylindrical control volume (m^2), Q_i is the advective flow rate through any slice of porous material i (m^3 h^{-1}), C_i is the cross-sectional area-averaged concentration at any given horizontal material slice i (μg m^{-3}) and P is the perimeter of the pore (m). Note that P is not a direct model input; $P\,\Delta y$ is the pore area in the control volume. It was assumed that advective flow is negligible through the material and that transport resistance to ozone reactions inside the porous network is negligible due to microscale path lengths. The latter assumption is explored in greater detail in the Supporting Information in Table S2; the result of assuming negligible transport resistance in pore volumes is that the total deposition velocity described by eq 1 simplifies to the surface deposition velocity, described by eq 4:

$$\frac{1}{v_d} = \frac{1}{v_s} = \frac{4}{\gamma_{ipa} < v >} \quad (4)$$

where v_s is the surface deposition velocity (m h^{-1}).

Equation 4 is applied in the discretized solution to eq 3 and the γ_{ipa} is assumed to be constant over the time period of material-ozone interaction. Reductions in uptake of ozone to materials with continued ozone exposure, or "aging", is documented in the literature. Experiments conducted previously attempted to minimize aging effects by conducting all trials with new materials and analyzing the first 1200 s of material-ozone interaction. If aging of test materials occurred on this time frame, the estimations of γ_{ipa} for new materials presented here would then represent underestimations of the true value of this parameter.

A flux-matching boundary condition is used at $y = 0$:

$$v_t(C_\infty - C_0) = \varepsilon\frac{D_e}{\frac{\Delta y}{2}}(C_0 - C_{y,1}) + v_d(1-\varepsilon)C_0 \quad (5)$$

The left-hand side of this equation describes ozone flux from bulk air through the boundary layer. Due to the immediate proximity of ozone molecules to the reaction sites at the boundary, v_d in eq 5 is determined using eq 4.

A no-flux boundary condition is used at $y = -h$:

$$D_e\frac{\partial C}{\partial y}\bigg|_{y=-h} = 0 \quad (6)$$

Equations 2, 5, and 6 were discretized in time, and eq 3 was discretized in time and space as described in eqs S1−S4 of the Supporting Information.

DOI: 10.1021/acs.est.5b00023
Environ. Sci. Technol. 2015, 49, 4398−4406

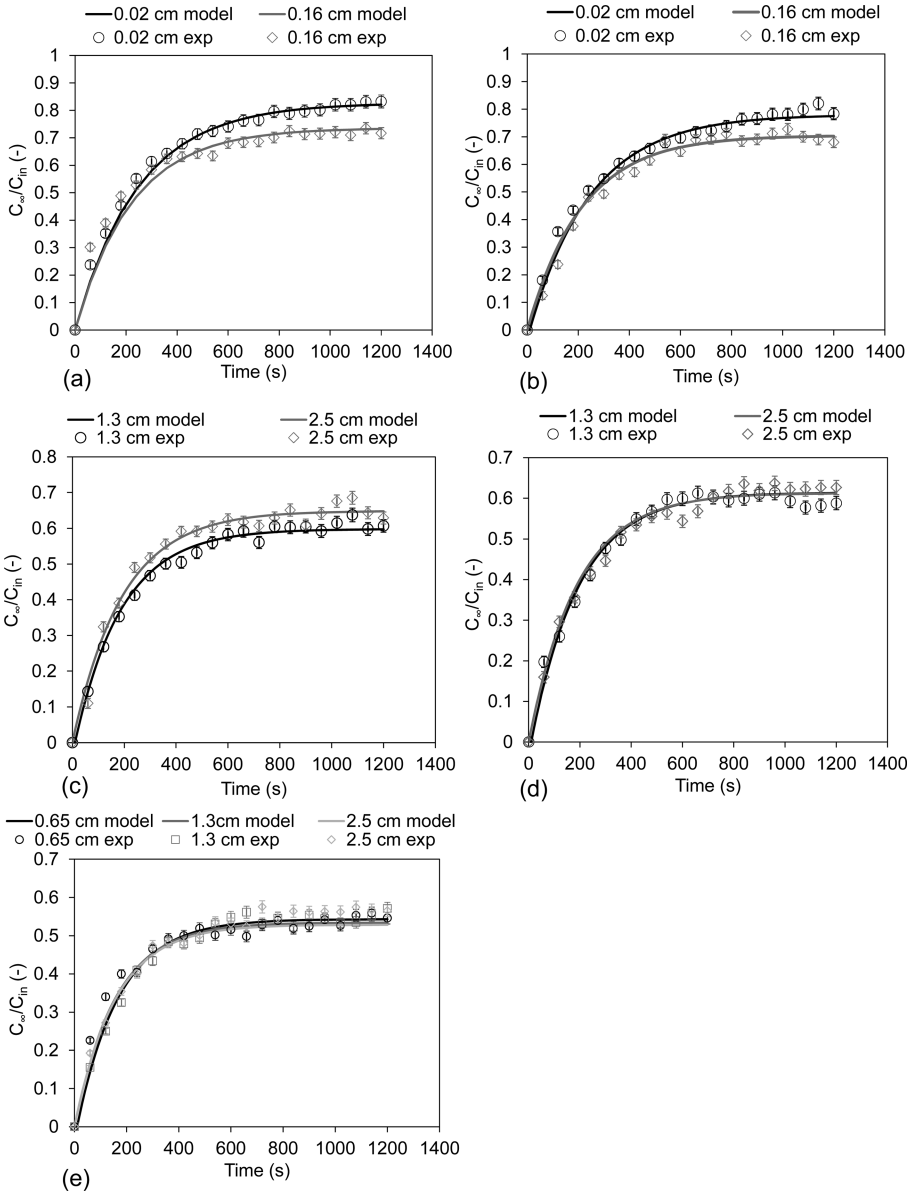

Figure 3. Predicted and experimental ratios of outlet and inlet ozone concentrations in chamber air for the five experimental materials. Plots (a) and (b) are cellulose paper filters, WF14 and WF15, respectively. Plots (c) and (d) are cementitious materials, pervious pavement (PP) and Portland cement concrete (PCC), respectively. Plot (e) is activated carbon cloth (ACC). Error bars in ozone concentration ratios correspond to the propagated uncertainty of the manufacturer-reported accuracy of the ozone analyzer (Model 205, 2B Technologies). Experimental data are shown at 60 s intervals for clarity; all analyses used the full experimental data set with 10 s interval.

Model Application. The discretized forms of eqs 2, 3, 5, and 6 were programmed in MATLAB (Mathworks, Inc.) and solved explicitly. The model was programmed to calculate the dynamic chamber concentrations of ozone from t = 0 s to t = 1200 s, with output in 10 s increments to match experimental output from a previous effort.[34] Each of the five materials was evaluated independently. The model end time (1200 s) was selected to allow sufficient time for the ozone concentration in the chamber to reach 99% of steady-state with only background losses and air exchange considered. Grid and time independence were tested by varying Δt and Δy until a nonchanging solution was achieved, defined here as a less than 1% change in predicted ozone concentration in the chamber air at t = 1200 s with a 50% reduction in time step or node spacing. Thicker materials (PCC, PP, and ACC) required modification of the code to incorporate a nonuniform grid of concentration nodes placed through the materials to support reasonable (<12 h) computational times. Each sample had a diameter of 15.2 cm. Pore diameters, d_p, were assumed to be the median pore diameter by volume for each material. The time step, Δt, was 0.025 ms for all scenarios. Modeled internal surface areas, SA_m (m^2), were estimated using the material volume (projected area multiplied by thickness), material porosity, and median pore diameter by volume using eq 7:

$$SA_m = \frac{4\varepsilon V}{d_p} \tag{7}$$

where all terms are as described previously.

A best-fit prediction of ozone concentration in chamber air was determined by varying γ_{ipa} input to the discretized forms of eqs 2, 3, and 5, recording the residual sum of squares, and repeating this process until the reaction probability with the

DOI: 10.1021/acs.est.5b00023
Environ. Sci. Technol. 2015, 49, 4398−4406

Table 1. Comparison of Reaction Probabilities Estimated with Resistance-Uptake theory (γ_{eff}) and with the Transport/Reaction Model Developed Here (γ_{ipa})

material	thickness, y (cm)	mass transfer coeff., v_t (cm s^{-1})	γ_{eff} (−), resistance uptake theory[a]	γ_{ipa} (−), this work	residual (ppb^2)	modeled internal surface area SA_m, (cm^2)	aerial projection of surface area (cm^2)
20−25 μm cellulose paper, WF14	0.02	0.14	1×10^{-6}	1×10^{-7}	652	8600	181
	0.16		6×10^{-6}	1×10^{-7}	2920	69 000	181
2.5 μm cellulose paper, WF15	0.02	0.14	1×10^{-6}	2×10^{-7}	688	7600	181
	0.16		1×10^{-5}	1×10^{-7}	773	61 000	181
pervious pavement, PP	1.3	0.22	2×10^{-5}	9×10^{-5}	477	890	181
	2.5		1×10^{-5}	6×10^{-6}	633	1800	181
Portland cement concrete, PCC	1.3	0.2	2×10^{-5}	2×10^{-5}	501	5.4×10^{11}	181
	2.5		2×10^{-5}	2×10^{-5}	606	1.1×10^{12}	181
activated carbon cloth, ACC	0.6	0.17	6×10^{-5}	6×10^{-7}	831	9100	181
	1.2		4×10^{-5}	4×10^{-7}	761	18 000	181
	2.5		5×10^{-5}	7×10^{-8}	315	36 000	181

[a]Values determined from experimental data[34] applied to resistance uptake theory[36] with a horizontally projected surface area. Average uncertainty in measurements of γ_{eff} across all materials is 26%.

minimum residual was determined. Estimates of γ_{ipa} ranging from orders of 10^{-3} to 10^{-9} were used to ensure that a global minimum total residual over a range of potential γ_{ipa} was achieved. Figure 2 shows an example of this total residual minimization process. The estimates of γ_{ipa} determined here are more physically accurate than models that rely on aerial projections of area as physical descriptors of materials; however, there remain a number of assumptions and limitations in the model as described in the Discussion.

Model sensitivity was characterized by conducting a deterministic sensitivity analysis through a process outlined by Jain and Singh[35] to assess the model response to changes in inputs that were experimentally determined. Low and high values of each input parameter were changed independently from their base case values and the impact on the steady-state concentration (C_∞ at t = 1200 s) was recorded. Sensitivity indices, SI, with units of change in output per change in input parameter x (ppb/[x]) and elasticity indices, EI (−), were calculated for nine experimentally determined model inputs according to eqs 8 and 9, respectively.

$$SI_{x-C_\infty} = \lfloor C_{\infty,1200s}(x_0 + \Delta x) - C_{\infty,1200s}(x_0 - \Delta x) \rfloor / 2\Delta x \quad (8)$$

$$EI_{x-C_\infty} = \lfloor x_0 / C_{\infty,1200s}(x_0) \rfloor SI_{x-C_\infty} \quad (9)$$

where x_0 is base case input variable and Δx is the change in input variable x.

The effect of an individual parameter's uncertainty on the uncertainty in γ_{ipa} was determined by estimating first the impact of a change of a parameter on $C_{\infty,1200\ s}$ using eq 10:

$$\Delta C_{\infty,1200s} = x_0(S_x) SI_{x-C_\infty} \quad (10)$$

Where S_x is the uncertainty associated with variable x.

The value of $\Delta C_{\infty,1200\ s}$ for each parameter, x_0, was used then to estimate the percent change in the modeled γ_{ipa} using eq 11:

$$\Delta\gamma_{ipa}(\%) = \frac{\left[-\left(\frac{\Delta C_{\infty,1200s}}{SI_{\gamma-C_\infty}} - \gamma_{ipa,0}\right)\right] - \gamma_{ipa,0}}{\gamma_{ipa,0}} \quad (11)$$

RESULTS

Model Results. The dynamic ratio of the outlet and inlet ozone concentration is shown in Figure 3; this ratio is related to the removal rate of ozone by the material, for example, a lower ratio indicates ozone is being removed at a higher rate. Estimates of γ_{ipa} to the test materials are shown in Table 1. Results in this section address a previously defined experimental condition where inlet flow was directed toward chamber walls.[34] Across the five materials, the model defined by eqs 2−6 is capable of accurately describing ozone concentrations in chamber air with varying material configuration; that is, the process of minimization of residual errors results in predicted chamber ozone concentrations that appear to agree with experimental concentrations. Experimental ozone concentrations in chamber air and model results for the two types of cellulose paper, WF14 and WF15, are shown in Figure 3 (a and b). The defining feature of these plots, compared to others shown in Figure 3, is a decrease in ozone concentrations in chamber air with increases in material thickness. For both thicknesses for both types of cellulose paper, the value of γ_{ipa} for which total residual is minimized ranges from 1×10^{-7} to 2×10^{-7}, with three of the four conditions being at the former value.

Pervious pavement (PP) and Portland cement concrete (PCC) are composed of similar raw materials, but differences in pore size distribution, porosity, and effective diffusion of ozone result in substantial differences in γ_{ipa}. In the 1.3 cm condition, PP had an γ_{ipa} of 9×10^{-5}, compared to 2×10^{-5} for PCC. The γ_{ipa} to PP is also greater than PCC in the 1.3 cm condition, but smaller in the 2.5 cm condition. The model developed in this work determined γ_{ipa} for PP in the 1.3 cm condition of 9×10^{-5}, more than an order of magnitude higher than the 2.5 cm condition (6×10^{-6}). The model developed in this work also determined a constant value of γ_{ipa} to PCC across thickness conditions, at 2×10^{-5}.

Estimates of γ_{ipa} determined for activated carbon cloth (ACC) are lower than values determined for cementitious materials, and averaged across thickness condition, similar to γ_{ipa} for cellulose filter papers (on the order of 1×10^{-7}). However, Figure 3(e) shows the smallest ratios of outlet and

DOI: 10.1021/acs.est.5b00023
Environ. Sci. Technol. 2015, 49, 4398−4406

inlet ozone concentration for activated carbon cloth, implying the importance of other factors for this material, such as internal diffusion and extent of interior surface area. Such factors may explain reductions in γ_{ipa} with increasing ACC thickness; γ_{ipa} decreased from 6×10^{-7} to 7×10^{-8} as thickness increased from 0.6 to 2.5 cm. For all five materials studied, implications of modeled values determined in this work and comparison with values determined with resistance-uptake theory are presented in the Discussion section.

Model Sensitivity and Uncertainty. The model described here relies on nine experimentally determined inputs. As a result, uncertainty propagates from each parameter to γ_{ipa}. Sensitivity and elasticity indices (SI and EI) describe the model response to a change in these inputs, and are provided in the si (Tables S3−S7) for each test material. The model was most sensitive (i.e., high EI) to parameters describing the inlet ozone concentration, the chamber flow rate and the material diameter. These parameters were all measured with instruments with 2% uncertainty or less (model 205 2B Technologies ozone monitor, FMA5400 Omega mass flow controller, and a vernier caliper, respectively). In contrast, the model was generally least sensitive to porosity and pore size, which we conservatively assumed to each have experimental uncertainty of 20%.[37,38]

We use the SI and uncertainty in each of the input parameters, reported in Supporting Information Tables S3−S7, to estimate the percent change in the modeled γ_{ipa} with eq 11. The uncertainties in γ_{ipa} derived from each input parameter are then summed in quadrature to estimate the total uncertainty associated with the model estimation of γ_{ipa}. Uncertainties associated with γ_{ipa} for WF14, WF15, PP, PCC, and ACC are ±47%, ± 48%, ± 1100%, ± 230%, and ±54%, respectively. For comparison, uncertainty in γ_{eff} ranged from 3% for 1.3 cm PCC to 28% for 0.02 cm WF14.[34]

DISCUSSION

Estimations of γ_{ipa}. A comparison of γ_{ipa} across materials and within a material at varying thickness illustrated improvements in material-ozone characterization for some materials, as well as challenges for future efforts for other materials. The model developed for this work results in consistent values of γ_{ipa} for cellulose paper (WF14 and WF15) at varying thickness. This represents an important improvement in modeling material−ozone interactions, as previous approaches result in increasing values of γ_{eff} with increasing thickness. Comparisons between WF14 and WF15 show similar ozone removal to filter paper with the change in manufacturer-specified particle diameter retention. This is likely a result of the identical chemical makeup of the materials as well as similar pore size distribution, porosity, and median pore diameter by volume determined for both types of filter paper.

Differences in modeled reaction probabilities between PCC and PP may be a result of modeled ozone concentrations for experiments with PP being insensitive to changes in γ_{ipa}. The EI for γ_{ipa} for PP is one to 2 orders of magnitude lower than for other test materials ($EI_{\gamma\text{-}C\infty} = -0.004$ for PP and ranges from −0.02 to −0.1 for other materials). This indicates that the model, when applied to PP, requires large changes in γ_{ipa} to substantially alter the modeled chamber ozone concentration. Conversely, small differences in chamber ozone concentrations result in large changes in γ_{ipa}. Modeling of PP is complicated due to the presence of millimeter-scale pores between mortar connected aggregate. The volume contribution from millimeter-scale pores results in a large median pore diameter by volume (Supporting Information Table S1) which discounts area contributions from nanometer-scale pores. A two-dimensional model of ozone transport and reaction may be required for materials such as PP with a large range of magnitudes of physical properties. Conversely, γ_{ipa} for PCC are consistent across material thickness conditions. This is logical given the low values of porosity, pore diameter, and effective diffusion coefficient determined for this material.[34] When combined with a large increase in thickness (thickness increases from 1.3 to 2.5 cm), relative to a material like cellulose paper (thickness increases from 0.02 to 0.16 cm), there is no resulting increase in reactive uptake from an increase in material thickness.

Unlike the materials discussed previously, the model estimates of γ_{ipa} for activated carbon cloth (ACC) decrease with increasing thickness, while Figure 3(e) shows stable ratios of outlet to inlet ozone concentration across thickness conditions. In theory, γ_{ipa} should be independent of thickness, implying the estimate of γ_{ipa} is impacted by other factors. Because the activated carbon is impregnated on a woven polyester backing, ACC has a unique combination of high internal surface area and high effective diffusion coefficient. Like the pervious pavement (PP), ACC has large, millimeter-scale pores in the woven backing and smaller micrometer- and nanometer-scale pores in the activated carbon media. Large pores present in ACC, a higher D_e, and a higher modeled internal surface area than PP contribute to a reduced estimate of γ_{ipa} by increasing the number of ozone molecule−surface collisions from accessible internal surface area through a greater depth of material. The model offsets this increase in molecule−surface collisions by reducing γ_{ipa} for an increase in depth. There are two potential explanations for this phenomenon: (1) the use of a median pore diameter by volume results in an underestimation of modeled internal surface area, leading to relatively fewer collisions (and therefore reactions) that create shallower concentration gradients through the material than exist in the model, but not in experimental conditions, or (2) an overestimation of the effective diffusion coefficient for activated carbon cloth.

Comparison with Resistance-Uptake Theory. Reaction probabilities accounting for internal pore area (γ_{ipa}) are generally 1−2 orders of magnitude lower than those determined with aerial projections of surface area (γ_{eff}, Table 1). The major factor contributing to this difference is the approach in accounting for surface area available for material-ozone interaction. The model developed here incorporates median pore diameters by volume on the order of micrometers to millimeters, resulting in a substantial increase in the modeled surface area compared to approaches using projected surface areas. Modeled internal surface areas are provided in Table 1, while projected surface areas used to determine γ_{eff} derive from a constant sample diameter of 15.2 cm.

As the thickness of the cellulose filters (WF14 and WF15) decreases from 0.16 to 0.02 cm, the filters more closely resemble the assumption of horizontally projected surface area of the resistance-uptake model, and the impact of internal surface area on material-ozone interaction is reduced. As a result, γ_{eff} and γ_{ipa} become more similar. In the 0.16 cm condition, γ_{ipa} are ∼50−100 × smaller than values determined with resistance-uptake theory, while in the 0.02 cm condition they are only 10× smaller. The comparison between γ_{eff} and γ_{ipa} made here for WF14 and WF15 appears in general agreement with a prior estimate of steady-state ozone reaction probabilities determined for calcium carbonate ($CaCO_3$) dust with

DOI: 10.1021/acs.est.5b00023
Environ. Sci. Technol. 2015, 49, 4398−4406

substantial internal pore area, and marble, a form of $CaCO_3$ taken to be nonporous; reaction probabilities determined for $CaCO_3$ as marble are 50−100 times smaller than those to dust,[39] a difference of similar magnitude to that observed here for WF14 and WF15 when internal pore area is accounted for in models of reactive uptake.

The modeled internal surface area for the 0.02 cm WF14 material was 8600 cm^2, compared to 181 cm^2 of projected surface area (similar results for the WF15 material). This 47-fold increase in surface area available for ozone-material interaction contributes to the reduction in γ_{ipa}. In the 0.16 cm WF14 condition, the model developed here accounted for 379 times more surface area than the resistance-uptake theory model. The factor of 10 and 50−100 difference between resistance uptake theory and reaction probabilities determined here for 0.02 and 0.16 cm conditions, respectively, indicate a nonlinear relationship between modeled internal surface area and reaction probability. This nonlinearity is likely due to lower ozone concentrations at greater depths in the material, lessening the importance of additional internal surface area added.

Estimates of γ_{ipa} to pervious pavement (PP) and Portland cement concrete (PCC) determined with resistance-uptake theory (γ_{eff}) are similar, in spite of a profoundly different material structure, a reflection of the statistically similar reductions in chamber inlet ozone concentrations shown in Figure 3(c) and (d) and a constant material sample size. Estimates of γ_{ipa} differ from γ_{eff} for PP and PCC, although with an inconsistent trend. The model insensitivity to PP reaction probability explains these mixed results. For PCC, a lower D_e, lower porosity, and smaller pore diameter than PP result in a steep concentration gradient through the material, with the majority of the depth of the material having a negligible ozone concentration. This results in modeled values of γ_{ipa} that are similar to the values determined using resistance uptake theory ($\gamma_{eff} = 2 \times 10^{-5}$ in both cases). Simmons and Colbeck[40] determined an ozone reaction probability based on the aerial projection of surface area (γ_{eff}) to outdoor concrete of 4×10^{-5}, a factor of only two higher than the estimate of γ_{ipa} determined for PCC here. The similarity in reaction probabilities between the model developed here and resistance uptake models using aerial projects of surface area suggests that for Portland cement concrete, surface reactions (that is, at $y = 0$) dominate.

Model estimations of γ_{ipa} to activated carbon cloth (ACC) determined in this work are approximately 2 orders of magnitude smaller than γ_{eff}. Grøntoft[16] present data used to calculate an effective reaction probability to an activated carbon cloth of 2×10^{-5}, larger than values predicted here for γ_{ipa} by approximately 2 orders of magnitude, but similar to values determined for γ_{eff}. This difference stems from a high effective diffusion coefficient through ACC, resulting in a flatter concentration gradient through the material and decreasing the modeled reaction probability determined in this work due to the modeled presence of greater effective, or accessible, internal surface area from increased transport in the axial direction.

For materials with consistent estimates of γ_{ipa}, inclusion of ozone diffusion and reaction through material substrates can also be considered in the context of previous work to estimate the Thiele modulus, which relates the rate of reaction to the rate of diffusion through the material substrate.[34] Reaction probabilities that account for internal surface area (γ_{ipa}) are most consistent across scenarios for WF14 and WF15, and both materials have low values of the Thiele modulus relative to other test materials. This implies internal diffusion is limiting when compared with internal reactions. Incorporating diffusive phenomena into the model appears to resolve the inconsistency in reaction probabilities determined across thicknesses with resistance-uptake theory (γ_{eff}) for WF14 and WF15. High values of the Thiele modulus for PCC mean internal diffusion occurs slower than internal reactions, implying reactions near the surface of this material are important. This is reflected in the similarity between γ_{ipa} and γ_{eff} for this material.

Impact of Changes in Fluid Mechanics. Indoor air velocities are variable, and thus the model was applied to an alternate experimental condition where the inlet port to the experimental chamber was oriented to directly impinge flow toward materials. On average, this change results in transport-limited deposition velocities (v_t) seven times higher than the original orientation where a tee union directed flow toward walls to drive circulation in the chamber. At high mass transfer, γ_{ipa} estimated for WF14, WF15, and PCC are 6×10^{-8}, 1×10^{-7}, and 7×10^{-7}, respectively. The model cannot determine a reaction probability that results in predicted values approximating experimental values for PP and ACC; in both cases experimental concentrations are lower than model concentrations for any value of reaction probability. This is likely a result of advection through large pores in these materials, a phenomenon not accounted for in the model.

The 0.2 cm WF14 condition at the high mass transfer condition showed reasonable agreement with the value reported in Table 1 for this work, while the same value was determined for WF15 under both low and high mass transfer conditions. Diffusive transport in the thin materials (WF14 and WF15) may be more competitive with advective transport over a smaller thickness than for the other test materials. The substantial difference between the γ_{ipa} determined under high and low mass transfer conditions in this work for Portland cement concrete (PCC) could result from two factors: (1) the model is sensitive to the mass transfer coefficient (EI = −0.26, see Supporting Information Table S6), and an overprediction of this parameter resulted in the model compensating by reducing γ_{ipa}, or 2) mass transfer to the material surface is advection based, resulting in transport to greater depths of the PCC material that result in increased material-ozone interaction not captured by the diffusion based model. More research is necessary to characterize the importance of advection through materials to satisfactorily model experimental scenarios with fluid flow directly impinging on materials.

Impact of Material Properties in an Indoor Environment. The model developed in this work can be applied to a larger scale indoor environment to illustrate the impact of materials and physical material properties on hypothetical ozone concentrations in a more realistic built environment. The modeled indoor concentrations of ozone can be used to determine the ozone removal effectiveness, or the percent removal of ozone in an indoor space resulting from the presence of a material, following previously defined protocols.[41] The hypothetical building used for this analysis is assumed to have an air exchange rate of 0.5 h^{-1},[42] a background ozone removal rate of 2.8 h^{-1},[43] and a transport limited deposition velocity of 0.14 cm s^{-1}. Introducing the WF14 cellulose paper in an indoor environment with a projected surface area coverage of 0.3 m^{-1} at thickness 0.02 cm increases building ozone removal effectiveness over baseline by 4%. Increasing thickness to 0.16 cm results in an increase of building ozone

DOI: 10.1021/acs.est.5b00023
Environ. Sci. Technol. 2015, 49, 4398−4406

removal effectiveness over baseline of 13%. Doubling the thickness of WF14, to 0.32 cm, results in an increase in ozone removal effectiveness over baseline by 14%. This shows that for WF14, transport and reaction in the material substrate beyond the depth of 0.16 cm results in a minimal increase in ozone removal effectiveness.

Sensitivity indices (SI) indicate the effect of a change in a material property on predicted ozone concentrations. The pore diameter has a positive SI, implying a decrease in this parameter will cause a decrease in predicted ozone concentrations (or increase in reactive uptake of ozone). This is because the pore diameter defines the availability of surface area in the internal material. Increasing surface area increases the number of material-ozone interactions, and at a constant reaction probability, the number of reactions. Model runs calculated with a 50% decreased value of d_p in the 0.02 cm WF14 scenario increase the ozone removal effectiveness in the hypothetical home from the baseline of 4−7%. The porosity, however, has a negative SI, implying an increase in this parameter will cause a decrease in predicted ozone concentrations. This is because an increase in porosity, at a constant pore diameter, increases the internal surface area by increasing the quantity of pores throughout the material. Increasing the porosity of WF14 by 20% results in an ozone removal effectiveness of 5%, an increase of only 1%.

Future research should focus on experiments and modeling on a wider array of materials with substantial surface area coverage in indoor environments, such as architectural coatings, ceiling materials, and floor materials. This may lead to an identification of opportunities for altering physical material properties to improve the ozone scavenging ability of widespread indoor materials. If accomplished in a manner that does not result in undesirable reaction products, such materials could be integrated into built environments to reduce occupant exposures to indoor ozone.

Study Limitations. The model presented in this work has a number of important limitations. The results presented here imply the model is most applicable to a scenario where diffusion occurs through pore spaces present in materials with steep pore volume distributions. The model only accounts for one-dimensional transport and neglects nonaxial diffusion that may be important for some materials. The one-dimensional diffusion assumption also discounts advective transport occurring above or into the material as well as scenarios where turbulent concentration boundary layers may affect mass transfer. To facilitate reasonable model solution times, a single value for pore diameter is used. The change in modeled γ_{ipa} due to a 50% change in input pore diameter ranges from 17% to 22% for WF14, WF15, PP, and ACC (Supporting Information Tables S3−S7), a range of uncertainty on modeled γ_{ipa} similar or slightly lower than other physical properties. In the case of PCC, the change in modeled γ_{ipa} is 0.4% for PCC (Supporting Information Table S6), a result of large modeled surface area and a small pore diameter. Diffusive flux through PCC is therefore limited as a result of low internal volume and removal near the surface, reducing the impact of uncertainty in pore diameter on the modeled γ_{ipa} for PCC. Exploratory model runs were conducted that partitioned material pore volumes into tertiles with accompanying values of pore diameter for each tertile input to the model, with negligible impact on modeled reaction probabilities. However, in these exploratory runs, molecular diffusion remained the sole mechanism of diffusive transport.

Future work should incorporate the full pore volume distribution determined via MIP and address the potential for advective flow and Knudsen and/or surface diffusion to impact material-ozone interactions in materials, particularly materials such as PP and ACC with complex pore structure. The development of an analytical solution to the equations presented here may facilitate such exploration while reducing the computational burden that would accompany the increase in model complexity. While a single value of pore diameter is not physically representative of material pore size distributions, model outcomes presented here show that it may be a reasonable approximation for materials with tighter cumulative pore size distributions (WF14, WF15, and PCC) and a limiting assumption for materials with a wider range of pore diameters (PP and ACC).

Since the model has one adjustable parameter, many assumptions and their effects, such as the presence of surface area beyond what is modeled due to the single pore diameter, are "lumped" into γ_{ipa}. Similarly, uncertainties associated with input parameters, such as porosity and background ozone loss, are propagated through the model and γ_{ipa}. Modeling efforts that include a fully independent estimate of the reaction probability are warranted given the complexity of many surfaces and the potential for greater understanding of indoor pollutant-material interactions. Highlighting specific material properties that improve the ability of materials to sequester or react with harmful pollutants may lead to greater incorporation of particularly effective types of materials in buildings and the development of materials with desirable pollutant removing physical properties.

■ ASSOCIATED CONTENT

Supporting Information

Additional information on input parameters, assumptions, and estimates of uncertainty for each test material is available free of charge via the Internet at http://pubs.acs.org.

■ AUTHOR INFORMATION

Corresponding Author

*Phone: 512-471-3611; fax: 512-471-0592; e-mail: corsi@mail.utexas.edu.

Notes

The authors declare no competing financial interest.

■ ACKNOWLEDGMENTS

This work was funded by a U.S. EPA Science to Achieve Results (STAR) Fellowship (#FP-91733001-0). We gratefully acknowledge many helpful discussions with Dr. Atila Novoselac regarding model development and implementation. ETG's efforts were also funded in part by the Republic of Singapore's National Research Foundation through a grant to the Berkeley Education Alliance for Research in Singapore (BEARS) for the Singapore-Berkeley Building Efficiency and Sustainability in the Tropics (SinBerBEST) Program. BEARS has been established by the University of California, Berkeley as a center for intellectual excellence in research and education in Singapore.

■ REFERENCES

(1) Bell, M. L.; Peng, R. D.; Dominici, F. The exposure-response curve for ozone and risk of mortality and the adequacy of current ozone regulations. *Environ. Health Perspect.* **2006**, *114*, 532−536.

DOI: 10.1021/acs.est.5b00023
Environ. Sci. Technol. 2015, 49, 4398−4406

(2) Ebi, K. L.; McGregor, G. Climate change, tropospheric ozone and particulate matter, and health impacts. *Environ. Health Perspect.* **2008**, *116*, 1449−1455.
(3) Devlin, R. B.; Duncan, K. E.; Jardim, M.; Schmitt, M. T.; Rappold, A. G.; Diaz-Sanchez, D. Controlled exposure of healthy young volunteers to ozone causes cardiovascular effects. *Circulation* **2012**, *126*, 104−111.
(4) Wolkoff, P.; Larsen, S. T.; Hammer, M.; Kofoed-Sørensen, V.; Clausen, P. A.; Nielsen, G. D. Human reference values for acute airway effects of five common ozone-initiated terpene reaction products in indoor air. *Toxicol. Lett.* **2013**, *216*, 54−64.
(5) Weschler, C. J. Ozone's impact on public health: Contributions from indoor exposures to ozone and products of ozone-initiated chemistry. *Environ. Health Perspect.* **2006**, *114*, 1489−1496.
(6) Chen, C.; Zhao, B.; Weschler, C. J. Assessing the influence of indoor exposure to "outdoor ozone" on the relationship between ozone and short-term mortality in U.S. communities. *Environ. Health Perspect.* **2012**, *120*, 235−240.
(7) Sabersky, R. H.; Sinema, D. A.; Shair, F. H. Concentrations, decay rates, and removal of ozone and their relation to establishing clean indoor air. *Environ. Sci. Technol.* **1973**, *7*, 347−353.
(8) Weschler, C. J.; Hodgson, A. T.; Wooley, J. D. Indoor chemistry: Ozone, volatile organic compounds, and carpets. *Environ. Sci. Technol.* **1992**, *26*, 2371−2377.
(9) Morrison, G. C.; Nazaroff, W. W. The rate of ozone uptake on carpets: Experimental studies. *Environ. Sci. Technol.* **2000**, *34*, 4963−4968.
(10) Kunkel, D. A.; Gall, E. T.; Siegel, J. A.; Novoselac, A.; Morrison, G. C.; Corsi, R. L. Passive reduction of human exposure to indoor ozone. *Build. Environ.* **2010**, *45*, 445−452.
(11) Gall, E. T.; Corsi, R. L.; Siegel, J. A. Barriers and opportunities for passive removal of indoor ozone. *Atmos. Environ.* **2011**, *45*, 3338−3341.
(12) Lamble, S. P.; Corsi, R. L.; Morrison, G. C. Ozone deposition velocities, reaction probabilities and product yields for green building materials. *Atmos. Environ.* **2011**, *45*, 6965−6972.
(13) Cros, C. J.; Morrison, G. C.; Siegel, J. A.; Corsi, R. L. Long-term performance of passive materials for removal of ozone from indoor air. *Indoor Air* **2012**, *22*, 43−53.
(14) Darling, E.; Cros, C.; Wargocki, P.; Kolarik, J.; Morrison, G. C.; Corsi, R. L. Impacts of a clay plaster on indoor air quality assessed using chemical and sensory measurements. *Build. Environ.* **2012**, *57*, 370−376.
(15) Klenø, J. G.; Clausen, P. A.; Weschler, C. J.; Wolkoff, P. Determination of ozone removal rates by selected building products using the FLEC emission cell. *Environ. Sci. Technol.* **2001**, *35*, 2548−2553.
(16) Grøntoft, T. Dry deposition of ozone on building materials. Chamber measurements and modelling of the time-dependent deposition. *Atmos. Environ.* **2002**, *36*, 5661−5670.
(17) Grøntoft, T.; Raychaudhuri, M. R. Compilation of tables of surface deposition velocities for O_3, NO_2 and SO_2 to a range of indoor surfaces. *Atmos. Environ.* **2004**, *38*, 533−544.
(18) Hoang, C. P.; Kinney, K. A.; Corsi, R. L. Ozone removal by green building materials. *Build. Environ.* **2009**, *44*, 1627−1633.
(19) Wang, H.; Morrison, G. C. Ozone-initiated secondary emission rates of aldehydes from indoor surfaces in four homes. *Environ. Sci. Technol.* **2006**, *40*, 5263−5268.
(20) Nicolas, M.; Ramalho, O.; Maupetit, F. Reactions between ozone and building products: Impact on primary and secondary emissions. *Atmos. Environ.* **2007**, *41*, 3129−3138.
(21) Nazaroff, W. W.; Gadgil, A. J.; Weschler, C. J. *Critique of the Use of Deposition Velocity in Modeling Indoor Air Quality*; ASTM International, 1993; pp 81−103.
(22) Reiss, R.; Ryan, P. B.; Koutrakis, P. Modeling ozone deposition onto indoor residential surfaces. *Environ. Sci. Technol.* **1994**, *28*, 504−513.
(23) Lee, P.; Davidson, J. Evaluation of activated carbon filters for removal of ozone at the PPB level. *Am. Ind. Hyg. Assoc. J.* **1999**, *60*, 589−600.
(24) Delage, F.; Pré, P.; Le Cloirec, P. Mass transfer and warming during adsorption of high concentrations of VOCs on an activated carbon bed: Experimental and theoretical analysis. *Environ. Sci. Technol.* **2000**, *34*, 4816−4821.
(25) Offermann, F. J.; Sextro, R. G.; Fisk, W. J.; Grimsrud, D. T.; Nazaroff, W. W.; Nero, A. V.; Revzan, K. L.; Yater, J. Control of respirable particles in indoor air with portable air cleaners. *Atmos. Environ.* **1985**, *19*, 1761−1771.
(26) Kwong, C. W.; Chao, C. Y. H.; Hui, K. S.; Wan, M. P. Catalytic ozonation of toluene using zeolite and MCM-41 materials. *Environ. Sci. Technol.* **2008**, *42*, 8504−8509.
(27) Axley, J.; Lorenzetti, D. Sorption transport models for indoor air quality analysis In *Modeling of Indoor Air Quality and Exposure*; Nagda, N. L., Ed.; ASTM International, 1993.
(28) Meininghaus, R.; Uhde, E. Diffusion studies of VOC mixtures in a building material. *Indoor Air* **2002**, *12*, 215−222.
(29) Marion, M.; Tiffonnet, A. L.; Santa-Cruz, A.; Makhloufi, R. Study of the resistances to transfer of gaseous pollutant between material and indoor air. *Build. Environ.* **2011**, *46*, 356−362.
(30) Hsu, I.; Masten, S. J. Modeling transport of gaseous ozone in unsaturated soils. *J. Environ. Eng.* **2001**, *127*, 546−554.
(31) Jung, H.; Kim, J.; Choi, H. Reaction kinetics of ozone in variably saturated porous media. *J. Environ. Eng.* **2004**, *130*, 432−441.
(32) Grøntoft, T. Measurements and modelling of the ozone deposition velocity to concrete tiles, including the effect of diffusion. *Atmos. Environ.* **2004**, *38*, 49−58.
(33) Morrison, G. C.; Nazaroff, W. W. The rate of ozone uptake on carpet: Mathematical modeling. *Atmos. Environ.* **2002**, *36*, 1749−1756.
(34) Gall, E. T.; Corsi, R. L.; Siegel, J. A. Impact of physical material properties on ozone removal by several porous materials. *Environ. Sci. Technol.* **2014**, *48*, 3682−3690.
(35) Jain, S. K.; Singh, V. P. *Water Resources Systems Planning and Management*; Elsevier, 2003.
(36) Cano-Ruiz, J. A.; Kong, D.; Balas, R. B.; Nazaroff, W. W. Removal of reactive gases at indoor surfaces: Combining mass transport and surface kinetics. *Atmos. Environ.* **1993**, *27*, 2039−2050.
(37) Hearn, N.; Hooton, R. D. Sample mass and dimension effects on mercury intrusion porosimetry results. *Cem. Concr. Res.* **1992**, *22*, 970−980.
(38) Cook, R. A.; Hover, K. C. Mercury porosimetry of hardened cement pastes. *Cem. Concr. Res.* **1999**, *29*, 933−943.
(39) Karagulian, F.; Rossi, M. J. The heterogeneous decomposition of ozone on atmospheric mineral dust surrogates at ambient temperature. *Int. J. Chem. Kinet.* **2006**, *38*, 407−419.
(40) Simmons, A.; Colbeck, I. Resistance of various building materials to ozone deposition. *Environ. Technol.* **1990**, *11*, 973−978.
(41) Miller-Leiden, S.; Lobascio, C.; Nazaroff, W. W.; Macher, J. M. Effectiveness of in-room air filtration and dilution ventilation for tuberculosis infection control. *J. Air Waste Manag. Assoc.* **1996**, *46*, 869−882.
(42) Yamamoto, N.; Shendell, D. G.; Winer, A. M.; Zhang, J. Residential air exchange rates in three major US metropolitan areas: Results from the relationship among indoor, outdoor, and personal air study 1999−2001. *Indoor Air* **2010**, *20*, 85−90.
(43) Lee, K.; Vallarino, J.; Dumyahn, T.; Ozkaynak, H.; Spengler, J. D. Ozone decay rates in residences. *J. Air Waste Manag. Assoc.* **1999**, *49*, 1238−1244.

DOI: 10.1021/acs.est.5b00023
Environ. Sci. Technol. 2015, 49, 4398−4406